The Structure of Water in Crystalline Aluminophosphates: Isolated Water and Intermolecular Clusters Probed by Raman Spectroscopy, NMR and Structural Modeling

Peter-Paul Knops-Gerrits,*,†,‡ Helge Toufar,§ Xiao-Yuan Li,|| Piet. Grobet,‡ Robert A. Schoonheydt,‡ Pierre A. Jacobs,‡ and William A. Goddard III*,||

Centrum voor Oppervlaktechemie en Katalyse, KU Leuven, Kardinaal Mercierlaan 92, B-3001 Heverlee, Belgium; Zeosorb Gmbh, Tricat-strasse, D-06749 Bitterfeld, Germany, Chemistry Department, Hong-Kong University of Science & Technology, Kowloon, Hong-Kong, Materials and Process Simulation Center (MSC), Beckman Institute, California Institute of Technology, Pasadena, California 91125

Received: March 3, 1999; In Final Form: July 14, 1999

Raman spectroscopy, thermo-gravimetry and NMR together with EEM-Monte Carlo calculations are used to elucidate the properties of water in Metavariscite, $AlPO_4$−H3, $AlPO_4$-8 and VPI-5. The framework density of the aluminophosphates decreases along this sequence, the pore size increases, and the water is less confined. The Raman vibrations of water in different aluminum phosphates reflects the polarization by Al and the number, and the type of hydrogen bonds in which they participate. Metavariscite and $AlPO_4$−H3 have well-defined symmetric ν_{OH} doublets in the region between 3000 and 3450 cm^{-1}, corresponding to structural water molecules. $AlPO_4$−H3 has additional free water with ν_{OH} at 3505 and 3563 cm^{-1}. In $AlPO_4$-8 and VPI-5 the majority of the water is zeolitic, and the corresponding feature is a broad band around 3200−3400 cm^{-1}. The differences between Al-coordinated and zeolitic water is also evidenced by EEM-Monte Carlo calculations. For the octahedral Al, ^{27}Al NMR is used to probe the different types involved. Mapping between principle hardness from electron population normal modes and force constants from the vibrational normal modes relates the influence of the environment of the water on the position and shape of the Raman bands. Perturbations imposed on water by the lattice Al (ν_{OH} < 3350 cm^{-1}) and H bonding by O atoms alone (ν_{OH} > 3400 cm^{-1}), change the symmetric OH-stretching polarization and decrease the principle hardness. The ν_{OH} vibrational frequency and the principal hardness splits as a result of different types of hydrogen bonding. When the number of interacting water molecules increases (Metavariscite → $AlPO_4$-H3 → VPI-5) a broadening of the Raman bands and the hardness distribution of the OH polarization is seen. This EEM-Monte Carlo approach is used for the semiquantitative interpretation of Raman data.

Introduction

The structure of water in different states, e.g., bulk water, water clusters, aqueous solutions of ions or organic molecules, and adsorbed water, has been a major research topic for years.[1] It is also a prime example of the fruitful combination of experimental and theoretical methods. Spectroscopic methods, such as IR,[2] Raman,[3] or NMR[4] spectroscopy can provide useful information about the local environment of water molecules. X-ray[5] or neutron[6] diffraction give information about the long-range arrangement of the water molecules. However, as a result of the poor long-range order of the above-mentioned systems, the derivation of structural models from the experimental data is not as straightforward as, e.g., in crystalline systems. Theoretical methods can be helpful here in two respects. Ab initio or semiquantitative calculations on water molecules in different environments assist in the interpretation of spectroscopic data.[7,8] Molecular modeling tools such as Molecular Dynamics or Monte Carlo simulation can generate reasonable models for the behavior of aqueous systems.[9,10]

In the present paper we focus on the interaction of water with crystalline aluminophosphates.[11,12] Unlike in zeolites,[13,14,15] water plays a crucial role within the crystalline lattice of aluminophosphates[16] since most of these structures are, in fact, $AlPO_4$ hydrates in which at least part of the aluminum occurs in octahedral $AlO_4(OH_2)_2$ coordination. In this case, two water molecules are bound to a framework aluminum in addition to four framework oxygen atoms. As a result, water in aluminophosphates usually exhibits a higher degree of order than in zeolites. This allows a more straightforward assignment of spectroscopic features to structural features.

The $AlPO_4$ structures under investigation cover a broad range of structural density and differ substantially with respect to the concentration of framework-bound and nonframework-bound water. Whereas Metavariscite[17] is an aluminum dihydrate, $AlO_4(OH_2)_2$ with Al-bound water, the $AlPO_4$-H3[18] contains alternating AlO_4 tetrahedra and $AlO_4(OH_2)_2$ octahedra linked by PO_4 tetrahedra. From the 1.5 molecules of crystal water per formula unit in $AlPO_4$-H3, 1.0 molecule is present in the form of aluminum dihydrate and 0.5 molecules are loosely held in the micropores. In VPI-5,[19,20] the Al atoms located between the double four-rings are aluminum dihydrate sites, representing one-third of the total aluminum content. Only two of the seven water molecules in the asymmetric unit of VPI-5 are bound to these sites. The remaining molecules are strongly organized in the 18-ring channels of VPI-5 in the form of a H-bonded triple helix. The $AlPO_4$-8[21,22] aluminum dihydrate occurs in one of the two types of 4.6.14 and 4^2.14 nodes. No information could

* To whom correspondence should be addressed.
† California Institute of Technology.
‡ Centrum voor Oppervlaktechemie en Katalyse.
§ Zeosorb Gmbh.
|| Hong-Kong University of Science & Technology.

10.1021/jp990817i CCC: $19.00
Published on Web 12/22/1999

be obtained about the structure of the non-Al-bound water in this case, probably due to the high degree of stacking disorder which leads pore blockage and hinders a regular occupation of all water adsorption sites.[23] Metavarisite, $AlPO_4$−H3, and VPI-5 can be synthesized by nearly identical procedures.[24,25] $AlPO_4$−H1 exhibits striking similarities with the VPI-5 structure.[26] Metavariscite and H3 are therefore often found as coproducts in VPI-5 synthesis.[27] The $AlPO_4$-8 is formed by structural transition of VPI-5, if the latter contains a high density of defects, upon thermal treatment.[28]

Raman spectra of the lattice vibrations of aluminum phosphates have previously been reported.[29] The features in the Raman spectra relate to the structural properties of the water molecules. In intermolecular hydrogen bonding (Y···HX), perturbations of the H-bonding by a group Y affects the HX stretch vibration.[30,31,32,33] Electron-acceptor neighbors (Z) that bind or ligate X (Y···HX···Z) such as coordinating ions or proton-donor groups also affect the HX stretch vibration.[1] The tight connection between the structure of water (experimental neutron diffraction O−H distances in liquid water are distributed around a well-defined peak at 1.85 Å at 277 K, consisting of about 1.8 H atoms at a distance of 2.35 Å and O−O distributions have a well defined peak at 2.975 Å consisting of 4.5 oxygen atoms at a distance of 3.3 Å from an oxygen at the origin (Oa)) and the appearance of the water O−H stretching spectra has been manifest from Raman studies on stoichiometric hydrates, chlathrathes and layered materials,[1] liquids,[3,34,35] and ice[36] or Infra-Red studies on gas-phase clusters.[4,37]

Here we present for the first time a systematic Raman study of the OH-stretching region in hydrated aluminum phosphates. To obtain more structural information, the Raman measurements were supplemented by other methods sensitive to the water structure such as XRD, DOR/MAS NMR, and DTA/DTG. Further evidence was obtained by a combined EEM-Monte Carlo calculation (EEM: Electronegativity Equalization Method)[38,39] and the Sensitivity Analysis (SA).[40,41] In that way, the properties of water molecules in different sites (charge, electronegativity, hardness) were calculated[42,43,44] and correlated with the spectroscopic data.[45,46]

Experimental Section

Synthesis. All syntheses were done using the following compounds: pseudoboehmite (Vista Chemicals), orthophosphoric acid (ACROS chimica, p.a. 85 wt % solution in water), deionized water, and dipropylamine (ACROS chimica, 99%).

VPI-5 was synthesized by a modified procedure of Davis et al.[47] The synthesis gel had the following molar composition

$$0.8\ Al_2O_3/1\ P_2O_5/1\ DPA/50\ H_2O$$

Dipropylamine (DPA) is used as the organic template. Pseudoboehmite was suspended in 25 parts of water and heated to 40 °C. The phosphoric acid was also diluted with 25 parts of water. After mixing both solution and suspension, the resulting gel was aged for 2 h. Then DPA was added. The synthesis mixture was autoclaved for 4−24 h at 135 °C. After crystallization, the samples were washed with water and dried at room temperature. Then they were treated under vacuum for 12 h at 20 °C and for 24 h at 100 °C, to avoid the irreversible transformation to $AlPO_4$-8.

$AlPO_4$-8 was obtained by heating VPI-5 at 150 °C for 24 h.

$AlPO_4$−H3 was synthesized by a method proposed by F. d'Yvoire.[48] In a closed vessel a mixture of diluted phosphoric acid, pseudoboehmite, and water with the molar ratios

$$0.38\ Al_2O_3/1\ P_2O_5/388\ H_2O$$

were refluxed for 48 h. The pH was held constant at 0.9. The precipitate was then washed and dried at 60 °C.

Metavariscite was obtained by the same procedure as $AlPO_4$−H3 but at drastically higher concentrations. The synthesis gel had the composition:

$$0.38\ Al_2O_3/1\ P_2O_5/110\ H_2O$$

Characterization Techniques. Solid State NMR. Prior to the measurement, the samples were placed in an NH_4Cl exsicator at room temperature for 24 h. The ^{27}Al magic angle spinning (MAS) NMR spectra were recorded on a Bruker MSL 400 spectrometer working at 9.4 T. A recycle delay of 0.1 s was used. Typically 3000 scans were accumulated. For the ^{27}Al double rotation (DOR) NMR measurements, the pulse length was 3 μs, corresponding to a flip angle of approximately 30°. A recycle delay of 1 s was used. The respective DOR probes used, the outer rotor spinning rate, and the number of scans (NS) for each spectrum are given as follows: VPI-5 (900 Hz Bruker probe, NS = 216); $AlPO_4$-8 (800 Hz Bruker probe, NS = 2000); $AlPO_4$-H3 (700 Hz Chemmagnetics probe, NS = 1000), Metavariscite (700 Hz Chemmagnetics probe, NS = 1000). The inner rotor spinning rate was 6 kHz.

X-ray Diffraction (XRD). X-ray diffraction patterns were recorded on a Philips HTK-KC diffractometer with a CuKα X-ray source, linked to a Philips 386 computer.

Scanning Electron Microscopy (SEM). SEM images were obtained with a JEOL Microprobe 733 after gold coating.

Thermogravimetric (TG) and Differential Thermo-Analysis (DTA). Thermogravimetric and differential thermal analyses were recorded on a Setaram TG-DTA 92 thermobalance using, typically, 30 mg of sample and a He flow of 35 mL/min. The temperature was increased at a rate of 5 °C/min from 20 to 800 °C.

Raman Spectroscopy. The Raman spectra were recorded on a Renishaw Raman Microscope. The zeolite samples, in powder form, were placed on a glass microscope slide. The power on the sample was about 2mW/mm^2. The collection time varied from sample to sample and was between 15 and 20 min. The spectra were background-corrected and a Fourier deconvolution procedure, described elsewhere,[3] was applied to resolve the overlapping bands in the OH stretching region.

Computational Methods. The Electronegativity Equalization Method (EEM) and a Sensitivity Analysis (SA) based thereon were applied to investigate the effect of the environment on the electronic properties of the water molecules inside the $AlPO_4$ structures. The EEM is derived from the Density Functional Theory (DFT).[49−56] It describes the energy of a system in atomic resolution as a function of the atomic charges

$$E = \sum_{i}^{m} \sum_{\alpha}^{n_i} \left(E^*_{\alpha_i} + \chi^*_{\alpha_i} q_{\alpha_i} + \eta^*_{\alpha_i} q^2_{\alpha_i} + \frac{q_{\alpha_i}}{8\pi\epsilon_0} \sum_{j}^{m} \sum_{\beta_j \neq \alpha_i}^{n_j} \frac{q_{\beta_j}}{R_{\alpha_i \beta_j}} \right) \quad (1)$$

where the summation runs over all atoms α in all molecules i. The functional dependence of the internal energy of each atom α on its atomic charge is characterized by the three coefficients E^*, χ^*, and η^*. These have been calibrated for several atom types so as to reproduce ab initio (STO-3G) charges (obtained by a Mulliken population analysis) and energies in a number of model compounds. The interatomic interactions are described by simple Coulomb interaction between the atomic charges. In infinite systems like, e.g., the crystalline aluminophosphates, the latter term has to be extended by a Madelung type summation.

The DFT states that in a molecule in its ground state the electronegativity, i.e., the derivative of the energy with respect to the electron density at a position r, has to be equal everywhere. Translated into the framework of EEM this means that the atomic electronegativities

$$\chi_{\alpha_i} = \left(\frac{dE}{dq_{\alpha_i}}\right)_v = \chi^*_{\alpha_i} + 2\eta^*_{\alpha_i} q_{\alpha_i} + \frac{1}{4\pi\epsilon_0} \sum_{j}^{m} \sum_{\beta_j \neq \alpha_i}^{n_j} \frac{q_{\beta_j}}{R_{\alpha_i \beta_j}} \quad (2)$$

have to be equal for all atoms in a molecule or any other subsystem i with free internal charge transfer. The electronegativity equation does not take effect, however, between subsystems i and j if no charge transfer is allowed, e.g., between two isolated molecules or between an adsorbent and a purely physisorbed adsorbate:

$$\chi_{i\alpha} = \chi_{i\beta} = \cdots = \chi_{i\omega} = \bar{\chi}_i \neq \chi_{j\alpha} = \cdots = \bar{\chi}_j \neq \bar{\chi}_m \quad (3)$$

On the basis of eqs 2 and 3 and taking into account that the sum of all atomic charges has to be constant, each subsystem can be described at the atomic level by the following matrix equation:

$$\begin{vmatrix} \eta_{\alpha\alpha} & \eta_{\alpha\beta} & \eta_{\alpha n} & -1 \\ \eta_{\beta\alpha} & \eta_{\beta\beta} & \eta_{\beta n} & -1 \\ & & & \\ \eta_{n\alpha} & \eta_{n\beta} & \eta_{nn} & -1 \\ 1 & 1 & 1 & 0 \end{vmatrix} \times \begin{vmatrix} q_\alpha \\ q_\beta \\ q_n \\ \bar{\chi} \end{vmatrix} = \begin{vmatrix} -\chi^*_\alpha \\ -\chi^*_\beta \\ -\chi^*_n \\ \bar{q} \end{vmatrix} \quad (4)$$

The elements of the matrix in eq 4, the so-called hardness kernels representing the second-order coefficients from eq 1, are given by

$$\eta_{\alpha\beta} = \left(\frac{d^2E}{dq_\alpha dq_\beta}\right)_v = \left(\frac{d\chi_\alpha}{dq_\beta}\right)_v = \begin{cases} 2\eta^*_\alpha & \text{if } \alpha = \beta \\ \dfrac{1}{4\pi\epsilon_0 R_{\alpha\beta}} & \text{if } \alpha \neq \beta \end{cases} \quad (5)$$

the quantities $\bar{\chi}$ and $\bar{q}$ are the equalized electronegativity and the total charge of the subsystem, respectively. Equation 5 contains the unknown atomic charges and the equalized electronegativity. It can be solved by inverting the matrix:

$$\begin{vmatrix} S'_{\alpha\alpha} & S'_{\alpha\beta} & S'_{\alpha n} & f_\alpha \\ S'_{\beta\alpha} & S'_{\beta\beta} & S'_{\beta n} & f_\beta \\ & & & \\ S'_{n\alpha} & S'_{n\beta} & S'_{nn} & f_n \\ -f_\alpha & -f_\beta & -f_n & \bar{\eta} \end{vmatrix} \times \begin{vmatrix} -\chi^*_\alpha \\ -\chi^*_\beta \\ -\chi^*_n \\ \bar{q} \end{vmatrix} = \begin{vmatrix} q_\alpha \\ q_\beta \\ q_n \\ \bar{\chi} \end{vmatrix} \quad (6)$$

The extension to systems containing more than one closed subsystem is straightforward. Equation 6 can be used to calculate charge distribution in the system as well as the electronegativity of the system. The elements of the inverted matrix contain additional information about the electronic properties of the system, the so-called sensitivity parameters. The internal softness kernels $S'_{\alpha\beta} = (dq_\alpha|d\chi_\beta)\bar{q}$ describe the internal charge redistribution caused by an external perturbation, the Fukui Indices $f_\alpha = (dq_\alpha/d\bar{q})$ describe the local effect of a charge transfer to and from the system and are considered as local reactivity indices for nucleophilic or electrophilic attacks. Finally, the global hardness $\bar{\eta} = (d\bar{\chi}/d\bar{q})$ is the resistance of the system against a charge transfer. The softness kernels form the internal softness matrix. Its eigenvectors are the normal modes of the electron redistribution (polarization) or the "electronic vibration" in analogy with the normal modes of the nuclear vibrations. The reciprocal eigenvalues of the internal softness matrix are called internal principal hardness values. They are formally analogous to the force constants of normal modes in the theory of molecular vibrations. It was shown recently that there exists a close relationship between the vibrational modes and the normal modes of the electron redistribution.[57,58] Generally, each vibrational normal mode is accompanied by one normal mode of the electron redistribution. The corresponding eigenvalues, i.e., the force constants and the internal principal hardness values are linked semiquantitatively. If an electron-redistribution mode becomes harder, the force constant of the corresponding vibrational normal mode will increase as well, resulting in a blue shift of the corresponding IR band.

As is obvious from eq 1, the EEM calculations require the knowledge of the position of each atom in the system. The calculations were done on the basis of crystallographic data given in the literature for metavariscite,[18] $AlPO_4$-H3,[19] and VPI-5.[17] The $AlPO_4$-8 was not included into the theoretical investigations since too little is known about the positions of the water molecules inside this structure. While the positions of the lattice atoms are generally well-known, with respect to the water molecules three situations can be encountered: (i) the positions of both the oxygen atom and the hydrogen atom are known from crystallographic studies (water in Metavariscite and water I and II in $AlPO_4$−H3, (ii) only the oxygen positions could be determined by diffraction methods (water III in $AlPO_4$−H3 and waters I−VI in VPI-5), (iii) the position of the water molecule is uncertain (water VII in VPI-5). In case (ii) the hydrogen atoms were added assuming a standard geometry for water (see Table 2); in case (iii) water molecules with standard geometry were placed initially on reasonable sites within the pore of the $AlPO_4$ structure. The position of these water molecules within the aluminophoshate was optimized subsequently using a combined Monte Carlo/EEM procedure.[50] In case (ii) only rotation around the center of mass was allowed while in case (iii) the molecule could move freely in the channel, including undergoing translation. This procedure followed a classical Metropolis algorithm using the total energy calculated by EEM as the criterion for the acceptance of MC steps. A *P*1 symmetry was assumed for the hydrogen positions. The simulation was performed at a temperature of 300 K in a canonical (NVT) ensemble until equilibrium was reached. Then, the temperature was reduced to 0 K and maintained at this until equilibrium. In the EEM/MC calculations no charge transfer was allowed between the different water molecules and between water molecules and the $AlPO_4$ structure. For the resulting structure, the atomic charges, the electronegativity of the water molecules and the aluminophosphate structure, the total energy of the system, and the interaction energies of the water molecules were calculated. The latter are defined as the sum of all electrostatic interactions of water molecules with all other atoms of the system. Furthermore, the above-mentioned sensitivity parameters, the normal modes of polarization of the system, and the corresponding internal principle hardness values were calculated. Thereby, we focused on the symmetrical O−H polarization of the water molecules which corresponds to the symmetrical O−H stretch vibration which was investigated by Raman spectroscopy in the present study.

Results

The synthesized products (Figures 1 and 2) are fine needles, associated as 'wheat-sheaves' in the case of VPI-5.[20,58,51,52] $AlPO_4$-8 forms irregular aggregates. $AlPO_4$−H1 is always contaminated with $AlPO_4$−H2[26] and other phases. For $AlPO_4$−

TABLE 1: Structural Parameters of the Alumino-Phosphates

IUPAC structure	symmetry	composition	framework density,[b] T-atoms/nm^3	window size (MR = member ring)[a]	pore/cage structure	T:O[c]	C:A[d]	ref
VFI (VPI-5)	P63	$AlPO_4 \cdot {}^7/_3(2)H_2O$	14.4	18 MR	1D tubular	2/1	2:5 (4)	49
AET ($AlPO_4-8$)	$Cmc2_1$	$AlPO_4 \cdot {}^nH_2O$	17.7	14 MR	1D tubular	2/1 (?)	2:n (?)	51
APC ($AlPO_4-H3$)	Pbca	$AlPO_4.1.5\ H_2O$	17.4	8 MR	2D tubular	1/1	2:1	52
Metavariscite	$P2_1/n$	$AlPO_4.2H_2O$	19.2			0/1	2:0	54

[a] The cross-sections for the windows are 1.25 nm (18MR), 0.79 × 0.87 nm (14MR), and 0.34 × 0.37 nm and 0.57 × 0.29 nm (8MR). [b] (tetrahedral + octahedral) sites/1000 Å^3. [c] Ratio between tetrahedral (T; $Al(IV)O_4$) and octahedral (O; $Al(IV)O_4(OH_2)_2$) coordinated aluminum in the framework. [d] Ratio between water in the first coordination sphere of framework aluminum (C) and adsorbed or occluded water (A).

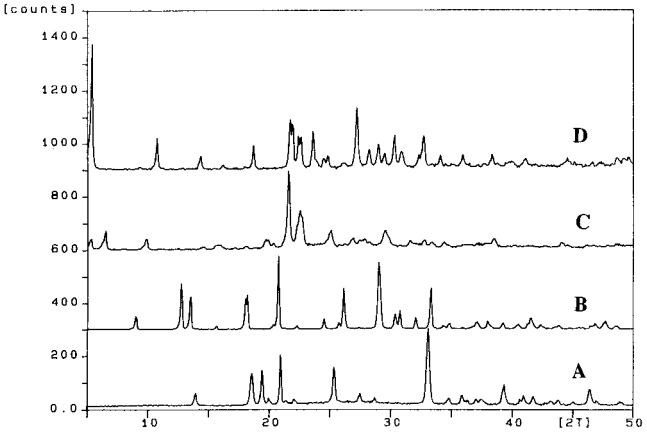

Figure 1. XRD of metavariscite (a), $AlPO_4-H3$ (b), $AlPO_4$-8(c) and VPI-5(d).

TABLE 2: Internal Geometry of the Water Molecules

	O−H1 (Å)	O−H2 (Å)	H1−O−H2 (°)	Δr
H_2O (standard) metavariscite	0.96	0.96	104	
H_2O (1)	0.84	0.81	110	0.03
H_2O (2)	0.85	0.86	110	0.03
$AlPO_4-H3$				
H_2O (1)	0.85	0.85	109	0.03
H_2O (2)	0.85	0.85	109	0.03
H_2O (3)	0.96	0.96	104	
VPI-5				
H_2O (1−7)	0.96	0.96	104	

H3, short prisms or thick plates with six to eight sides were obtained. The prisms or plates are stacked in piles. Metavariscite forms fibers of a few millimeters, either isolated or associated in radial structured spheres. The formation of variscite occurs when the solutions are more diluted than in the case of metavariscite. The crystallinity of the as-synthesized samples was confirmed by XRD (Figure 1). No amorphous or crystalline impurities (e.g., $AlPO_4$-11 in the samples of VPI-5) are present.

Thermoanalytical data are shown in Figure 3. Most water leaves the structure between 20 and 180 °C, except for metavariscite that still loses water at higher temperatures. Total amounts of lost water are 20.5, 19, 20, and 15% for metavariscite, $AlPO_4-H3$, VPI-5, and $AlPO_4$-8, respectively. Only for metavariscite different dehydration steps are clearly discerned: 7% to 115 °C, the amount decreasing with increasing crystallization time. The structural water within the metavariscite lattice is lost in two equal steps at 170 °C and subsequently at 215 °C. From the structural data water with two strong single hydrogen bonds is more strongly withheld than water with two bifurcated hydrogen bonds. This is followed by a gradual weight loss of 3.5% to 800 °C with a structure conversion to $AlPO_4$ tridymite at 500 °C. $AlPO_4-H3$ shows minor dehydration at

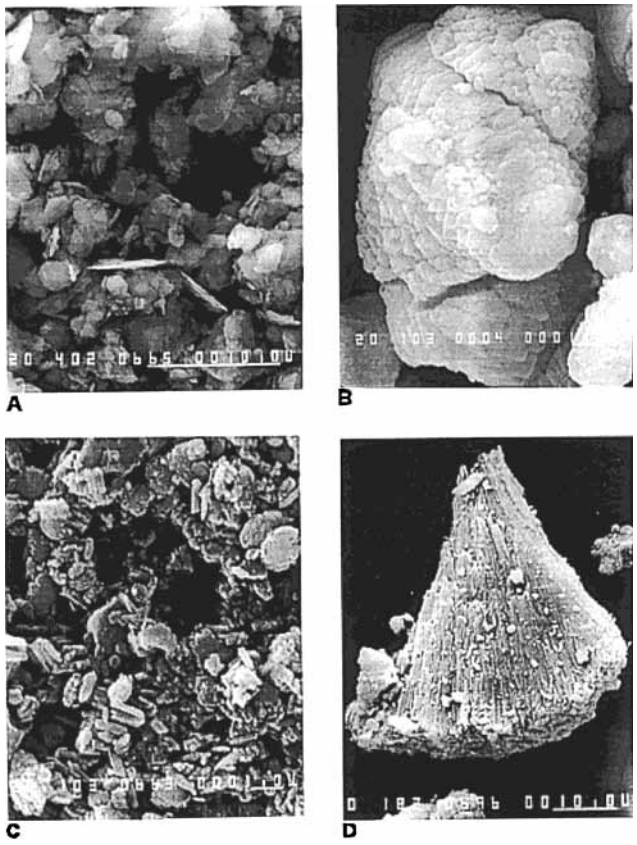

Figure 2. SEM of metavariscite (a), $AlPO_4-H3$ (b), $AlPO_4$-8(c) and VPI-5(d).

50 °C of adsorbed water; the structural water, bound to octahedral Al and bound to the lattice by hydrogen bonding, leaves the structure around 125 °C leading to a transition to $AlPO_4-C$ that at 200 °C transforms in $AlPO_4$-D.[41,57] VPI-5 shows a more gradual dehydration in three steps. Water leaves the 18MR (1.25 nm) channels at 40, 95, and 110 °C. Three types of water are removed from the three-water-layer "onion-skin", leading to the structural collapses into $AlPO_4$-8. The water nearest to the framework is harder to remove than that near the center of the cavity. In $AlPO_4$-8 dehydration maxima occur at 40, 80, and 95 °C. From VPI-5, more water desorbs than from $AlPO_4$-8, the strength of binding is also higher for VPI-5 then for $AlPO_4$-8.

Solid State MMR Spectroscopy. The ^{27}Al MAS NMR spectra of the four samples in Figure 4 show that the ratio of octahedral versus tetrahedral Al follows the sequence: metavariscite 100%, $AlPO_4-H3$ 50%, VPI-5 (or $AlPO_4-H1$) and $AlPO_4$-8 33%.

The ^{27}Al MAS NMR spectrum of metavariscite shows double chemical shift (−10.8 and −8.4 ppm) in the octahedral Al

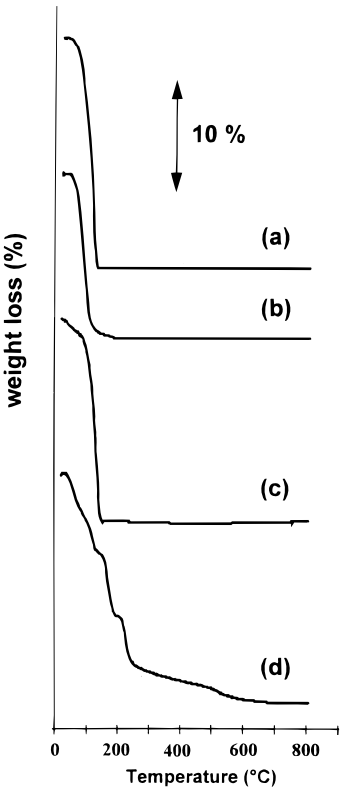

Figure 3. TGA plots of VPI-5(a), $AlPO_4$-8(b), $AlPO_4$−H3(c) and metavariscite(d).

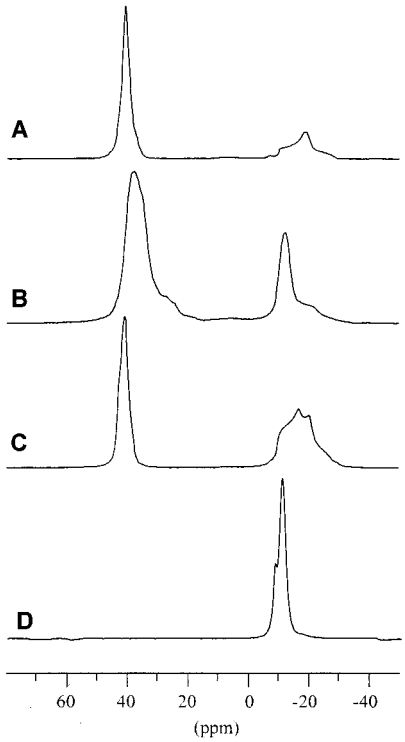

Figure 4. ^{27}Al MAS NMR spectra of VPI-5(a), $AlPO_4$-8(b), $AlPO_4$−H3(c) and metavariscite(d).

region. When the spinning rate is increased from 5 to 12 kHz the latter peak becomes dominant. For longer crystallized samples with less superficially associated water the peak at −8.4 ppm is absent at 5 kHz and only appears at 12 kHz. Double rotation (Figure 5) gives a broadened −10.8 ppm line with two asymmetric spinning sidebands. The nature of the broadening will further be discussed.

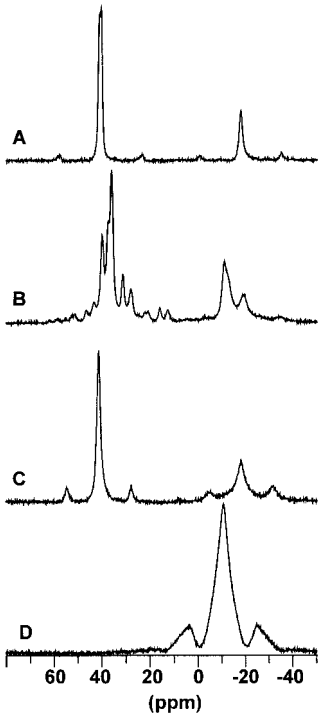

Figure 5. ^{27}Al DOR NMR spectra of VPI-5(a), $AlPO_4$-8(b), $AlPO_4$−H3(c) and metavariscite(d).

The ^{27}Al MAS NMR spectrum of $AlPO_4$−H3 is characterized by both a tetrahedral (41.2 ppm) and octahedral Al signal (−12.6, −16.6, and −20.0 ppm). In double rotation (Figure 5) the octahedral line at −18.2 ppm is well-resolved, due to the suppression of quadrupole interactions. The tetrahedral line is again seen at 41.2 ppm.

In view of the fact that $AlPO_4$-8 has 5 crystallographic T-sites the ^{27}Al MAS NMR spectrum is poorly resolved with two broad lines at 38.2 and −12.1 ppm of, respectively, tetrahedral and octahedral Al. However, the DOR spectrum in Figure 5 gives, after deconvolution into Gaussian lines, 5 tetrahedral ^{27}Al lines (39.7, 37.4, 35.9, 31.1, 27.9) and 4 octahedral ^{27}Al lines (−11.2, −13.3, −15.6, −19.4 ppm). Owing to the rotation-synchronized experiments, only even-spinning sidebands appear at 61.6, 58.2, 55.1, 52.9, 51.0 ppm and 24.5, 21.8, 20.4, 15.7, 12.5 ppm.

In agreement with literature NMR data and with crystallographic data for VPI-5,[53] two tetrahedral Al sites occur in the six-member rings (6MR) and one octahedral Al site in the four-member rings (4MR). In ^{27}Al MAS NMR, the octahedral signal occurs at 41.1 ppm, that of tetrahedral Al at −19 ppm; and the DOR spectrum exhibits three peaks at 41.2, 40.4, and −18.4 ppm in a 1:1:1 ratio.[54]

Raman Spectroscopy. The Raman spectra of the OH stretching region (3000−3800 cm^{-1}) are presented in Figure 6. The band maxima are summarized in Table 3. The Raman spectrum of **metavariscite** is characterized by two sharp bands at 3110 and 3374 cm^{-1}, the former with an ill-defined low-frequency shoulder around 3000 cm^{-1} (at 3008 cm^{-1}) and the latter with a well-defined shoulder at 3437 cm^{-1}. Both sharp bands correspond to $AlO_4(OH_2)_2$ associated water, with hydrogen bonding to lattice oxygen atoms. The region above 3500 cm^{-1}, where O−H stretching vibrations of free water oscillators are generally found, is clear of Raman bands since there is no channel structure or free void volume to contain free water.

In **$AlPO_4$-H3** spectra, three broad low-frequency bands are observed at 3379, 3225, and 3020 cm^{-1} which can be assigned to $AlO_4(OH_2)_2$ associated water. The doublet consisting of very

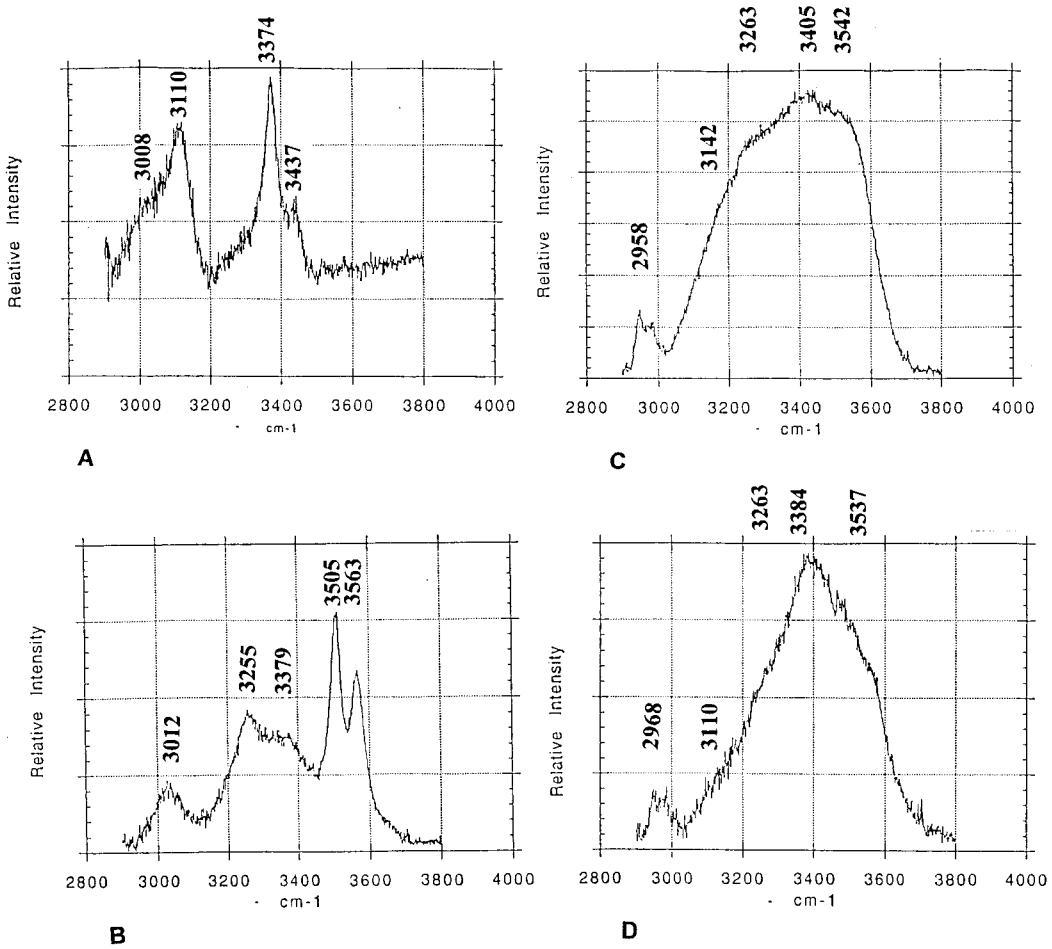

Figure 6. Raman Spectra of the O−H stretching vibrations in the 3000−3800 cm^{-1} region of metavariscite (a), $AlPO_4$−H3 (b), VPI-5 (c) and $AlPO_4$-8(d).

TABLE 3: Raman OH-Stretching Frequencies

IUPAC structure	water donor OH-stretching band positions					
VFI (VPI-5)	2958	3142 (sch)	3263		3405	3542
AET (AlPO4−8)	2968	3110 (sch)	3263	3384		3537 (sch)
APC (AlPO4−H3)	3012		3255	3379 (sch)		3505 (s) 3563 (s)
metavariscite	3008	3110 (s)		3374 (s)	3437 (sch)	none

sharp bands in the region at about 3505 and 3563 cm^{-1} can be associated with the water molecules in the channel.

The spectra of $AlPO_4$-8 and VPI-5 both have broad asymmetric bands with maxima at 3400 cm^{-1}. For **$AlPO_4$-8**, the most prominent band in the spectrum is at 3384 cm^{-1} and a second at 3263 cm^{-1}. The 3110 and 3537 cm^{-1} shoulder has, respectively, a lower and a higher intensity compared with those for VPI-5. In **VPI-5**, the 3405 cm^{-1} band is prominent; the 3263 cm^{-1} band (with a 3142 cm^{-1} shoulder) and 3542 cm^{-1} band are of higher intensity than those for $AlPO_4$-8. The spectra of the large-pore molecular sieves $AlPO_4$-8 and VPI-5 are less structured, showing bands over a much broader frequency range than those of the denser Metavariscite and $AlPO_4$−H3.

Computations. The structure of metavariscite, including the water positions as taken from the literature,[18] is shown in Figure 7. There are two types of water present in the metavariscite structure differing in the way the hydrogen atoms interact with the aluminophosphate lattice. For type 1 (red), both hydrogen atoms interact with one lattice oxygen each with distances typical for hydrogen bonds (1.8−1.9) as shown in part B of Figure 7. For type 2 (dark blue), both hydrogen atoms interact with two lattice oxygen atoms each with somewhat bigger distances (2.1−2.4 Å, see part C of Figure 7). The hydrogen−oxygen bonds within the water molecules are considerably smaller than those of the free water molecule (0.84−0.86 Å vs 0.96 Å). According to the accuracy of the structure refinement, this bond shortening should be significant, while the differences between the molecules of type 1 and type 2 and especially the asymmetry of the type 1 are within the margins of error. To separate the effect of the internal water geometry from the influence of the environment, i.e., the interaction with the $AlPO_4$ lattice, a number of additional calculations were done (i) assuming a standard geometry for the water molecules and the orientation as derived from the crystallographic data and (ii) assuming a standard geometry of the water molecules but after a re-optimization of their orientation via the EEM/MC procedure. Finally, the EEM calculations were also done on free water molecules with the bond lengths and angles found in the metavariscite structure. The results are summarized in Table 4.

For $AlPO_4$-H3 (Figure 8) only the orientation of the "free", i.e., non Al bound water (type 3, dark blue), had to be optimized by the EEM/MC procedure. The resulting structure is in close agreement with the symmetry of the framework (*Pbca*). The water molecules of Al bound types 1 (red) and 3 form a chain along the 8-ring channel of $AlPO_4$−H3 with a hydrogen of type 1 pointing to an oxygen of type 3 with an intermediate hydrogen bond distance (1.95−2.1 Å) and hydrogen of type 3 pointing to lattice oxygen with somewhat larger distances (∼2.25 Å, see

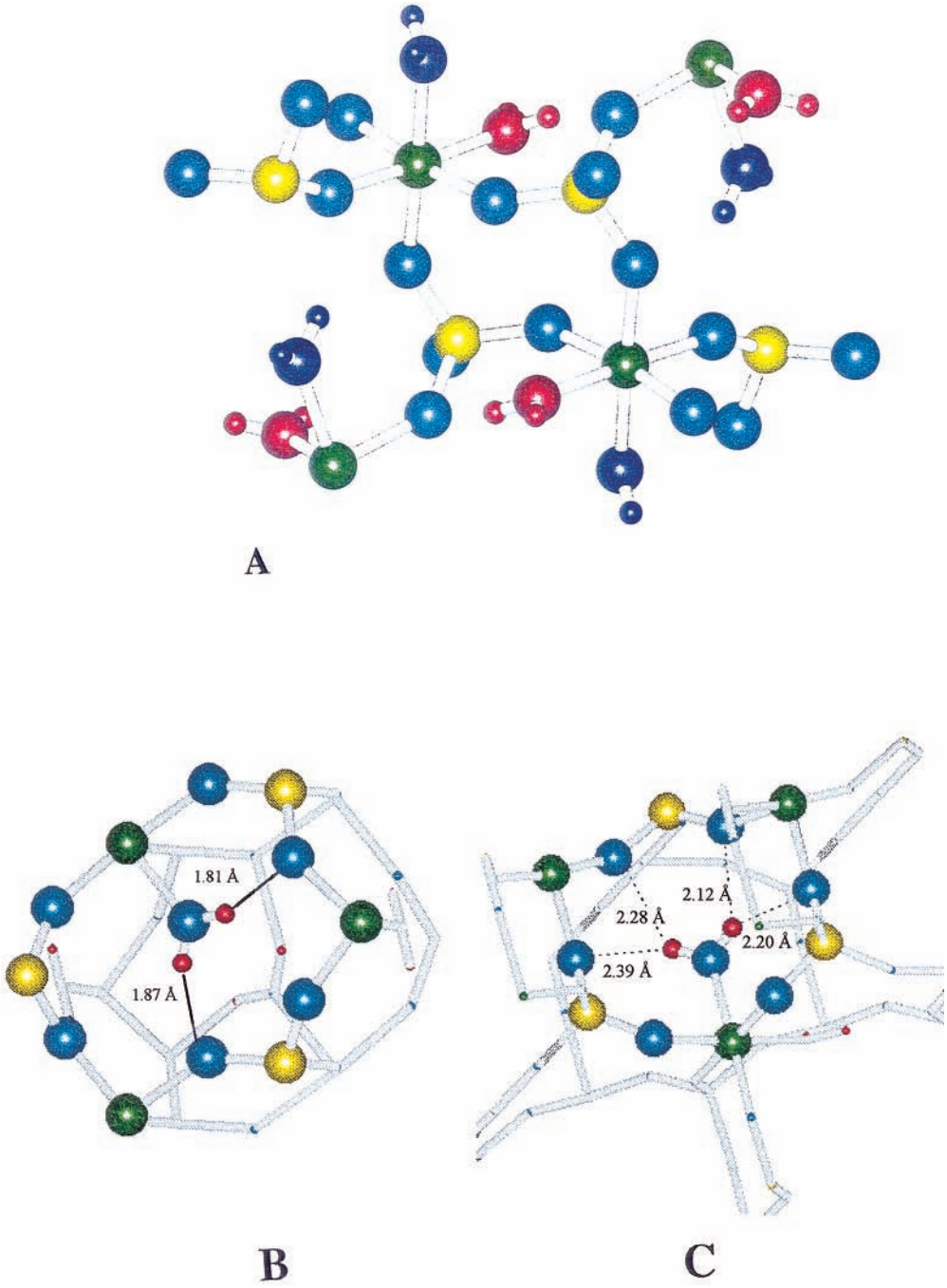

Figure 7. EEM optimized structures of metavariscite (overview A, B, and C).

parts B and C of Figure 8). The molecules of type 2 stick into the 6-rings, and the hydrogen atoms are solely bound to lattice oxygen atoms (1.8 and 2.0 Å, respectively, see part D of Figure 8). Again, the crystallographic data result in intramolecular O−H bond distances of about 0.85 Å. This bond shortening is significant, as well, and in good agreement with the results for metavariscite. The electronic properties of the lattice and the different water molecules were calculated on this structure. They are shown in Table 5.

The VPI-5 structure (Figure 9) required an optimization of the orientation of the water molecules 1−6 and a full optimization, i.e., including translation, for the type 7 ones. Figure 9 shows the resulting arrangement of the water molecules in the channel of VPI-5. As expected, structural disorder increases when going from the wall of the channel toward the center. The Al bound water molecules of type 1 (green) and type 2 (red) obey the lattice symmetry nearly perfectly. For the first shell of the non Al bound water molecules (type 3, blue and type 6, yellow), some slight deviations occur. The deviations from the lattice symmetry are more pronounced for the second shell (type 4, magenta and type 5, cyan) while the central molecules (type 7, orange) are distributed in the remaining void space in disordered fashion. Since no hydrogen positions could be determined for the water in VPI-5 all calculations were done assuming the standard geometry. The resulting electronic properties can be found in Table 6.

Discussion

Prior to a quantitative discussion of the calculated electronic properties, one has to assess the role of the internal geometry of the water molecules. As stated above, changes in the geometry of the water molecules found in the $AlPO_4$ structures

TABLE 4: EEM Parameters in Relation to the Water Structure in MV

	crystal				water		
metavariscite	E (eV)	χ (V)	q (e)	η_{O-H}(V/e)	χ (V)	q (e)	η_{O-H}
$H_2O(1)$	1.56	5.34	$q_O = -0.92$ $q_{H1} = 0.44$ $q_{H2} = 0.48$	3.88−3.96	5.48	$q_O = -0.64$ $q_{H1} = 0.31$ $q_{H2} = 0.34$	4.26
$H_2O(2)$	1.16	5.41	$q_O = -0.76$ $q_{H1} = 0.38$ $q_{H2} = 0.38$	4.56−4.67	5.48	$q_O = -0.55$ $q_{H1} = 0.27$ $q_{H2} = 0.28$	4.93
$AlPO_4$ structure		3.22	$q_{Al} = 1.39$ $q_P = 1.56$ $q_O = 0.73-0.74$				

	relaxed position				free water		
	E (eV)	χ (V)	q (e)	η_{O-H}	χ (V)	q (e)	η_{O-H}
$H_2O(1)$	1.19−1.30	5.56−5.75	$q_O = -0.58$ to -0.59	5.68−5.94 6.70−6.79	5.76	$q_O = -0.38$ $q_{H1} = 0.19$ $q_{H2} = 0.19$	7.13
$H_2O(2)$	1.15−1.17	5.85−5.92	$q_O = -0.57$ to -0.58	5.68−5.94 6.70−6.79			
$AlPO_4$ structure		3.17	$q_{Al} = 1.37$ $q_P = 1.56$ $q_O = 0.72-0.74$				

compared with those of free water molecules occur after coordination. In crystalline hydrates O−H bond distances of as little as 0.89 Å are reported.[55] Furthermore, from the general bond-length variation rules for electron donor−acceptor interaction stated by Gutmann[56] one would expect a bond lengthening rather than a shortening. While there is some indication that the interaction of a water molecule with a highly charged electron acceptor could course a considerable bond shortening,[57] the formation of hydrogen bonds with other water molecules or lattice oxygen can result in a lengthening of as much as 0.1 Å. In the present case both effects should compensate each other at least partially. Therefore, the observed bond shortening seems to be at least somewhat exaggerated. The results in Table 4 allow estimation of the contribution of the bond shortening to the change of the electronic properties. The contraction of the water molecule, as such, results in a change in the polarization, a slightly lower electronegativity, and a much lower principal polarization hardness than that in the standard water. One has to notice here, however, that these effects are probably strongly exaggerated. The calculations were performed with a single set of parameters derived for standard geometry, i.e., a bond distance of 0.96 Å in the case of water. It is to be expected that these parameters, especially the atomic hardness, are dependent on the bond distance. More specifically, the atomic hardness will increase when the bond distance is shortened, thereby reducing the observed effects. The crystalline environment also causes a stronger polarization compared with that of the corresponding isolated water and a decrease of the principle hardness, i.e., both the change in the internal structure and the environment have, qualitatively, the same effect. A quantitative discussion is, however, limited because of the uncertainty about the real extent of the bond length contraction and the effect of the latter on the electronic properties.

In AlPO−H3 the same trends are observed for the aluminum-bound water molecules. In this case, due to the similar internal geometry, the polarized modes are coupled for all of these water molecules even if the crystallographic geometry is used in the calculations. The third type of water, which is only hydrogen-bound with the structure, exhibits a much lower interaction energy and principal hardness which are only slightly lower than those in the free water molecule. The same is found for VPI-5. There is a clear gap between these quantities for Al bond and non Al bond water, but no further differentiation within these groups. However, because of the greater number of molecules in the unit cell and the wider variety of chemical environments, the distribution of principal hardness is much broader. This is illustrated in Figure 10 for the three structures discussed here in comparison with different water clusters.

The extent of the water coordination to Al is determined by ^{27}Al NMR via the fraction of octahedral Al. For metavariscite only the latter is observed. In the literature metavariscite ^{27}Al MAS NMR spectra are symmetrical with a chemical shift of −13.2 ppm (4.7 T), whereas for most other $AlPO_4$ materials they are asymmetrical.[58] When [^{1}H-^{27}Al] CP-MAS NMR is employed, the strongly cross-polarized ^{27}Al produces a sharp chemical shift at −12.4 ppm (4.7 T). These values mediate the values of −7.6 ppm for coordination to three PO_4 tetrahedra and three water molecules in $Al(H_2O)_3(H_2PO_4)_2(HPO_4)$ and that at −16.6 ppm for Al coordinated to six PO_4 tetrahedra in $Al(H_2PO_4)_3$.[59] When this structure retains superficially adsorbed water both in ^{27}Al MAS NMR spectra and [^{1}H-^{27}Al] CP-MAS NMR, an additional chemical shift appears; in ^{27}Al DOR NMR spectra a broadening is seen. This extra shift (MAS) and the broadening (DOR) is indicative of the presence of a second type of octahedral Al that has different dipolar interactions, due to outer-sphere interactions of superficially adsorbed water, not canceled in the DOR experiment. DOR only enhances spectral resolution when line widths are mainly related to quadrupolar interactions. Poor crystallization or samples in a vitreous state give the result that all species are subjected to a continuous distribution of local surroundings which broadens the lines, e.g. in ^{27}Al DOR NMR spectra of cloverite, lines are as broad as in ^{27}Al MAS NMR.[70] As a result of high dipolar interactions in this very dense structure and not extremely high quadrupolar interactions the double speciation thus results in a broadening of the ^{27}Al DOR NMR spectra.[60]

For $AlPO_4$−H3, the ^{27}Al MAS NMR[61] signal and it's shape, consisting of different maxima, can be attributed to octahedral coordinated Al being subjected to quadrupolar interaction in an electrostatic field deviating from axial symmetry. In the ^{27}Al DOR NMR such effects of quadrupolar interactions are lifted, and a single peak is seen for the octahedral Al. The alternation between tetrahedral and octahedral coordinated Al is confirmed by the 1:1 ratio of the intensities of the two signals, in the ^{27}Al MAS NMR spectra. [^{1}H-^{27}Al] CP MAS NMR shows

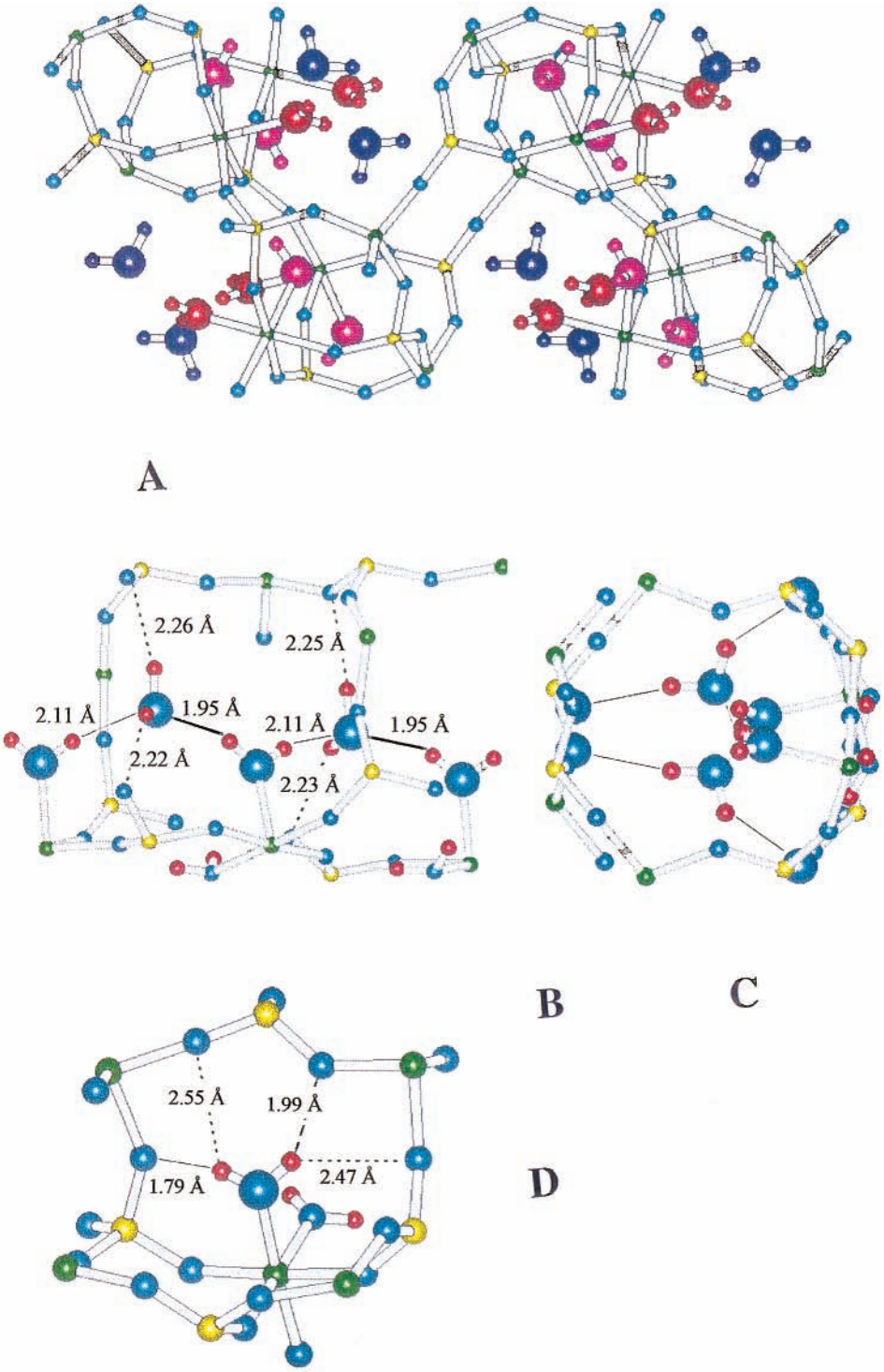

Figure 8. EEM optimized structures of $AlPO_4$-H3 (overview A, B, C, and D).

both signals indicating that the protons are close to Al and that the octahedra are part of the structure.[62]

For $AlPO_4$-8, five different crystallographic T-atoms are present. The observed chemical shift for the tetrahedral signal is 38.2 ppm whereas that of octahedral aluminum is −12.1 ppm. Previously by ^{27}Al MAS NMR[63] on $AlPO_4$-8 the five types of T-atoms were assigned, and by ^{27}Al DOR NMR[64] the presence of the these five types was verified by deconvolution of the DOR NMR into five Gaussian lines for the tetrahedral and four Gaussian lines for the octahedral sites. The average water content can be predicted from summation of the ^{27}Al NMR intensities of the octahedral aluminum Gaussian lines to be around 30%, or there are almost 3 hydrated T-atoms in the 14MR per nine T-atoms (See Figure 4 for the 5 tetrahedral and 4 superposed tetrahedral types).

For VPI-5, there are three different crystallographic aluminum sites, two (two-thirds of total amount) in the six-member rings and another (one-third of total) between two four-member rings.[55] The deconvolution of the ^{27}Al DOR NMR in the case of VPI-5 thus shows three Gaussian lines, two for the tetrahedral and one for the octahedral aluminum.[65] From the ^{27}Al NMR intensities, 33% of the Al is octahedral.

Raman-spectra of aluminum phosphates in the OH stretching region in combination with EEM calculations give structural

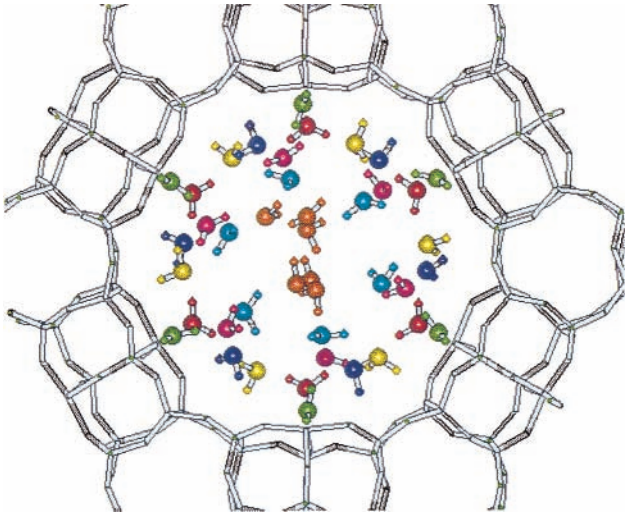

Figure 9. EEM optimized structure of VPI-5.

TABLE 5: EEM Paramaters in Relation to the Water Structure in $AlPO_4$−H3

	crystal			
$AlPO_4$−H3	E (eV)	χ (V)	q (e)	η_{O-H}(V/e)
$H_2O(1)$	1.12	5.45	$q_O = -0.77$ $q_{H1} = 0.39$ $q_{H2} = 0.38$	4.37 − 4.68
$H_2O(2)$	1.30	5.50	$q_O = -0.79$ $q_{H1} = 0.39$ $q_{H2} = 0.40$	4.37 − 4.68
$H_2O(3)$	0.37	5.09	$q_O = -0.46$ $q_{H1} = 0.23$ $q_{H2} = 0.23$	6.92 − 7.09
$AlPO_4$ structure		3.44	$q_{Al} = 1.38$ (T) $q_{Al} = 1.42$ (O) $q_P = 1.66$ (1) $q_P = 1.70$ (2) $q_O = 0.74-0.80$	

information about water siting. Lattice O atoms (polarized by Al) or structures in which water is positioned so as to give short O··O distances result in hydrogen bonding. Experimental O−O distances in liquid water are 2.759 Å at 223 K, 2.840 Å at 277 K, and 2.975 Å at 298 K, consisting of about 4.5 O at a distance of 3.3 Å. Binding of water with lattice Al affects the electronic properties of interacting water molecules much stronger than the formation hydrogen bonds with other water molecules. It causes strong polarization of the O−H bond and a dramatic increase of the principal hardness of the symmetric O−H polarization. These effects cause a decrease of the force constant of the O−H bond leading to a downshift of the Raman band. Although hydrogen bond formation has qualitatively the same effects, the polarization is less pronounced. When the O··O bond lengths are above 3.5 Å no hydrogen bonding occurs, and Al polarization effects, alone, affect OH properties for water that has hydrogen entirely localized on one water molecule.

It is known that the intramolecular and the intermolecular coupling of OH oscillators are nearly equal in strength in crystalline ices in low-density amorphous solid water, and in liquid water. In low-density amorphous solid water two kinds of disorder appear: the distribution of protons is disordered and an 8° distribution of O··O··O angles is seen. There are many studies of the rate of change of the OH frequency with the average O··O separation.[34,35] A literature reference gives $d\upsilon/dRoo = 1843$ cm^{-1}/Å for Roo = 2.76 Å.[34] The Raman OH stretching of ice Ih at 3100 cm^{-1} has a frequency and width

TABLE 6: EEM Parameters in Relation to the Water Structure in VPI-5

VPI-5	E (eV)	χ (V)	q (e)	η_{O-H}(V/e)
$H_2O(1)$	0.94−1.04	5.8−6.1	$q_O = -0.55(1)$ $q_{H1} = 0.28(1)$ $q_{H2} = 0.27(1)$	5.71−5.90 8.34−8.66
$H_2O(2)$	0.78−0.87	5.3−5.7	$q_O = -0.53(1)$ $q_{H1} = 0.27(2)$ $q_{H2} = 0.26(1)$	5.71−5.90 8.34−8.66
$H_2O(3)$	0.29−0.32	5.1−5.6	$q_O = -0.45(05)$ $q_{H1} = 0.23(1)$ $q_{H2} = 0.22(1)$	6.16−6.98
$H_2O(4)$	0.20−0.29	5.0−5.4	$q_O = -0.44(1)$ $q_{H1} = 0.22(1)$ $q_{H2} = 0.22(1)$	6.16−6.98
$H_2O(5)$	0.25−0.35	4.7−5.3	$q_O = -0.44(2)$ $q_{H1} = 0.22(1)$ $q_{H2} = 0.22(1)$	6.16−6.98
$H_2O(6)$	0.28−0.36	5.1−5.6	$q_O = -0.44(2)$ $q_{H1} = 0.22(1)$ $q_{H2} = 0.22(1)$	6.16−6.98
$H_2O(7)$	0.26. 0.38	5.1−5.5	$q_O = -0.44(2)$ $q_{H1} = 0.22(1)$ $q_{H2} = 0.22(1)$	6.16−6.98
$AlPO_4$ structure		3.49	$q_{Al} = 1.46$ (O) $q_{Al} = 1.43$ (T1) $q_{Al} = 1.36$ (T2) $q_P = 1.76$ (1) $q_P = 1.81$ (2) $q_P = 1.75$ (3) $q_O = 0.75-0.84$	

increase with temperature and a growth of intensity in the 2800−3000 cm^{-1} region.[35]

From our experimental data a rough division can be made between the zone for water <3350 cm^{-1} where Al influences the OH stretch and the zone >3400 cm^{-1} which is not directly affected by Al. A downshift in the OH stretch frequency thus indicates hydrogen is delocalized through Al polarization. Further splitting occurs due to different kinds of hydrogen bonding and/or due to intermolecular coupling in analogy with the spectra of water in small clusters. The O··O bond distances for Al−O_w-H··O−Al increase from 2.67 for MV to 2.89 for $AlPO_4$−H3; these are absent in VPI-5,[17] thus only for MV these types of water molecules with delocalized hydrogen bonds are expected. For $AlPO_4$−H_3, the 2.60 Å distance between an aluminum-bound lattice oxygen and a free, but very confined, nonaluminum-bound water molecule, i.e., Al−O_l··H−O_w−H shows the effect of Al on O··O distances; analogously 2.57 and 2.59 Å distances are seen for Al−O··H−O_w−H bonds in VPI-5.[17] For the free water in VPI-5 that forms helices, analogous O··O distances are seen of 2.78 Å in H−O_w−H··O_w−H interactions.[17]

For metavariscite two sharp bands of $AlO_4(OH_2)_2$ associated OH stretches co-occur, at 3110 and 3374 cm^{-1}, and these can be related to Al bound water molecules closely bound with two lattice oxygen atoms by two hydrogen bonds (of 1.81 and 1.87 Å) or in which the two OH stretches are involved in bifurcated hydrogen bonding to four lattice oxygen atoms (2.12, 2.20, 2.28 and 2.39 Å). Thus lattice O are involved in hydrogen bonding with the Al associated water belong to different $AlO_4(OH_2)_2$ octahedra (Figure 7). The 3437 cm^{-1} shoulder may result from partial intramolecular coupling in the water molecule involved in bifurcated hydrogen bonding. The interaction is promoted by the equal strength in these two oscillators involved in bifurcated H-bonding. The shoulder at 3008 cm^{-1} may result from Al bound stretches, from a predominantly single donor stretch, due to a low percentage of imperfect siting. In this region for all the AlPO structures a comparable band is seen. In MV

TABLE 7: ^{27}Al MAS NMR and ^{27}Al DOR NMR Chemical Shifts (ppm) of the Aluminum Phosphates

sample	NMR	tetrahedral Al					octahedral Al			
MV	MAS	none					−10.8	−8.4		
	DOR	none					−10.8			
$AlPO_4$−H3	MAS	41.2					−12.6	−16.6	−20.0	
	DOR	41.2					−18.2			
$AlPO_4$−8	MAS	38.2					−12.1			
	DOR	39.7	37.4	35.9	31.1	27.9	−11.2	−13.3[a]	−15.6[a]	−19.4
VPI-5	MAS	41.1					−19.0			
	DOR	41.2	40.4				−18.4			

[a] From deconvolution.

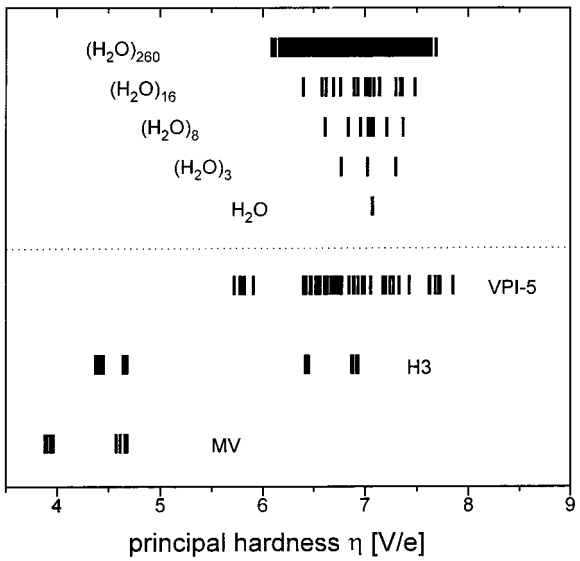

Figure 10. Principal hardness of the symmetric O−H polarization for water in aluminophosphates compared with water in clusters of different size.

there is no channel structure or free void volume to contain free water, and thus, above 3500 cm^{-1} no O−H stretching vibrations of free water oscillators are found.

In $AlPO_4$−H3 spectra, one of the three bands, observed at 3379 cm^{-1} closely resembles that in metavariscite since it results from Al bound water that shows hydrogen bonding to four lattice oxygen atoms of which two, at 1.79 and 1.99 Å, are close. $AlO_4(OH_2)_2$ associated water which does not show hydrogen bonding to lattice oxygen atoms but to oxygen atoms of the third water type (1.95 and 2.11 Å apart) may result in a band at 3225 cm^{-1}. The precise siting in the small channel-like voids of $AlPO_4$−H3 clearly defines interactions of non Al bound water molecules with their surroundings (Figure 8). These water molecules show interactions both through their O with two H atoms of water molecules bound to Al (1.95 and 2.11 Å apart) and through their two H atoms with two lattice O atoms (2.2−2.23 and 2.25−2.26 Å apart). This is a crystallographic clear case of a molecule in which the two O−H stretches are involved in a double donor interaction with two lattice oxygen atoms. Correspondingly, the doublet consisting of very sharp bands in the region above 3500 cm^{-1}, ∼3505 and 3563 cm^{-1}, can be associated to double O−H donor stretching oscillators. The most plausible explanation for the significant splitting observed for this doublet, −58 cm^{-1}, is the intramolecular interaction,[3] promoted by the almost equal strength of the H bonds for the two oscillators of the water molecule, correlating with their almost equal length.

In other $AlPO_4$ structures the band pattern is broadened. When the channels are wider, water molecules show an increased mobility, resulting in a bandwidth increase (Figure 10). Continuum-broadening generally results from the embedding of a state in the vibrational continuum of states which lie below it. In-homogeneous broadening results from imperfect siting or temperature variations in the local environment.

The Raman spectra of $AlPO_4$-8 and VPI-5 are very similar except for the differences in the intensities (and some of the positions) of the corresponding bands. For $AlPO_4$-8, the low intensity of the shoulder at 3110 cm^{-1} of the $AlO_4(OH_2)_2$ associated water with very strong hydrogen bonding, results from the different way in which Al is bound with water molecules before and after the structural transition and the difference in interaction of coordinated water molecules with those of the next shell. The double-donor OH stretches of the $AlO_4(OH_2)_2$ associated water with a vibration at 3263 cm^{-1} are not directed toward lattice oxygen atoms, since the separation between an aluminum-coordinated water molecule and a lattice oxygen is large to be bridged in this structure. The prominent 3384 cm^{-1} band can either be assigned to water OH stretching vibrations of single hydrogen-bound water molecules in the channel or to doubly hydrogen-bound aluminum-associated water, since the band is situated in the spectral transition region between both species. As a result of the size of the channels of $AlPO_4$-8, both single- and double-donor hydrogen-bound water molecules can be expected. The latter hydrogen-bound double-donor water in the channels is observed as the shoulder at 3537 cm^{-1}.

The 3263 cm^{-1} band with a 3142 cm^{-1} shoulder of VPI-5 is of much higher intensity than the comparable 3263 cm^{-1} band with a 3110 cm^{-1} shoulder in the $AlPO_4$-8 structure. In ice, the OH band covers the region between 3100 and 3300 cm^{-1}, typical for very strong hydrogen bonds. The water molecules located within the main 18 ring appear to form a series of three layers, which are organized in a helical form, from the framework atoms toward the center of the pore. They form a weak H-bound network in which the five free and the two lattice-bound (one interacts stronger than the other) water molecules participate. From the references, the water−water distances observed in ice (O−H···O distance of 2.77 Å[20,34,35]) and inside the channels of VPI-5 (O−H··O distance of 2.78 Å[20]) are similarly short. The Raman bands can be ascribed to single-donor and double-donor O−H bonds, respectively. However, in the literature, upon refinement of the VPI-5 structure, sensible convergent positions are obtained, which reflect the highly ordered structure of the water molecules in the channel.[17−20] Such strong H bonding, in layer or helixlike structures, points to bands at 3142 and 3263 cm^{-1} in analogy to the strength of the bands in ice. Here, especially in the region defined for Al-polarization of the O−H stretch (Table 3), short water O−H stretches are obtained without Al polarization within the helical layers it forms in the VPI-5 structure.

In analogy to $AlPO_4$-8, the 3263 cm^{-1} band is one of $AlO_4(OH_2)_2$ associated water with double-donor bonding to water in the wide channels and either moving in-phase or out-of-phase.

The important 3405 cm^{-1} band is associated with the single hydrogen-bound stretch vibration in the channel. The 3542 cm^{-1} band in VPI-5 is of higher intensity then the shoulder at 3537 cm^{-1} in $AlPO_4$-8 with relative intensities of 0.82 and 0.53, respectively. In the helical layers water molecules are linked in chains. In these water molecules one hydrogen is involved in hydrogen bonding in a linear array;[20] the other hydrogen can either not interact with other water molecules (dangling ends) or undergo hydrogen bonding within the layer structure. Such nonaluminum-bound water shows Raman bands in this region.

Single- or double-donor hydrogen bonding is a function of the binding distance. Whereas for aluminum-bound water low-lying single-donor stretch vibrations (lowest between brackets) occur for MV (3008 cm^{-1}) and $AlPO_4$−H3 (3012 cm^{-1}), for $AlPO_4$-8 (2968 cm^{-1}) and VPI-5 (2958 cm^{-1}) they are ultimately redshifted. Double donor stretch vibrations are present for MV (3110−3374 cm^{-1}), $AlPO_4$−H3 (3255−3379 cm^{-1}), $AlPO_4$-8 (3110−3263 cm^{-1}), and VPI-5 (3142−3263 cm^{-1}). Short stretches for water in the helices in VPI-5 like those in ice are not affected by aluminum polarization. The layered association causes a change in the number of single- versus double-donor stretching modes in the structure. For "free" water low-lying single-donor stretch vibrations are not seen for MV and $AlPO_4$−H3, but are seen (lowest between brackets) for $AlPO_4$-8 (3384 cm^{-1}) and VPI-5 (3405 cm^{-1}), and double-donor stretch vibrations are absent for MV and are present for $AlPO_4$−H3 (3505−3563 cm^{-1}), $AlPO_4$-8 (3537 cm^{-1}), and VPI-5 (3542 cm^{-1}). The complexity arising from co-occurrence of different possible stretching modes can only be untangled on the basis of a clear model of the individual structures.

Conclusions

This work demonstrates the use of Raman spectroscopy combined with EEM/SA structure optimization in the characterization of water structures in aluminum phosphates. The physical models of the association of water with the lattice and other molecules can be obtained from Raman, TGA, XRD, and NMR data of the structures. In aluminophosphates different interactions are defined:

(1) Lattice aluminum can coordinate water, binding it through its oxygen, in the octahedral $AlO_4(OH_2)_2$ in the structure. In more dense structures it can only give hydrogen bonding to the lattice, in less dense structures it can interact with free water molecules through hydrogen bonding, but not with the lattice. (2) Nonlattice associated water molecules can coordinate through oxygen and hydrogen. Since oxygen is not bound to aluminum it can complete or partial hydrogen bonds can be formed either with polarized lattice-bound or free water molecules. Hydrogen bonding via hydrogen is analogous to the previous case, occurring with lattice oxygen atoms or free water molecules. (3) Lattice oxygen within the structure can take over the hydrogen-bonding acceptor function. The absence (or very limited number) of acceptor water molecules in the lattice structure results in a different spectral appearance from water cluster systems.

The O−H polarization effect, observed in the Raman spectra, can be divided between the zone <3350 cm^{-1} where aluminum influences the symmetric stretch and/or water is strongly hydrogen-bound (i.e., in a helical structure) and the zone >3400 cm^{-1} where water molecules are not present in the first shell around aluminum. In the EEM data, this division is again seen: the hardness h_{OH} is below 6 for the aluminum coordinated water; it is higher than 6 if the water molecules are not associated with lattice aluminum. A 400 cm^{-1} downshift corresponds to a drop in h_{OH} by about 2−3 V/e for the symmetric stretch frequency upon aluminum coordination. In TGA aluminum-bound water is only released above 100 °C, for MV at about 170 °C and 215 °C, whereas for $AlPO_4$-H3 it is at about 125 °C.

Analogous to the division between single and double donor OH-stretching vibrations made for water in small clusters,[2−38] it is clear from the Raman data that an analogous division is possible for the Al bound and the nonAl bound water. Whereas this division for free water molecules is likely around 3450−3550 cm^{-1}, for the aluminum bound molecules it is expected to occur at 3050−3150 cm^{-1}. The broadness of the principal hardness region $\Delta\eta_{OH}$ for the OH stretch is a measure for the number of modes that participate in the continuum forming the bond. If more geometries co-occur, an increase of $\Delta\eta_{OH}$ and broadening of the band is observed (Figure 10).

Water hydrogen bound with the structure exhibits a much lower interaction energy compared with aluminum bound water. The principal hardness decreases only little from free to lattice hydrogen bound water molecules; it is however severely lowered for aluminum-bound water molecules. There is a clear gap between these quantities for aluminum-bound and "free" water, but no further differentiation within these groups. For a greater number of molecules in the unit cell and a wider variety of chemical environments, the distribution of the principal hardness is much broader as illustrated in Figure 10 for the structures discussed here in comparison with different water clusters.

The combination between the structural information (XRD, EEM/SA) and information on the hardness of the OH stretching vibration thus give valuable information to predict the Raman data. This combined characterization in combination with thermogravimetric and NMR data give a complete image of the structure of water in the aluminum phosphate structures.

Acknowledgment. The authors acknowledge IUAP-PAI sponsoring from the Belgian Federal Government. The authors would like to thank Prof. J. Martens for stimulating discussions, Prof. W. Viaene for the X-ray diffraction measurements, Dr. V. Zhelyaskov for help with Raman, and Mr. J. Nickolov for providing the software for Fourier self-deconvolution. P.P.K.G. thanks the Belgian National Fund for Scientific Research (NFWO) for a fellowship as postdoctoral researcher, H.T. thanks the European community for a fellowship in the framework of the Human Capital and Mobility program, X.Y.L. thanks the Research Grant Council from HKUST for financial support, WAG thanks BP Amoco for financial support.

References and Notes

(1) Franks, F. *Water: A Comprehensive Treatise;* Plenum Press: New York, 1972−1979; six volumes.

(2) Pribble, R. N.; Zwier, T. S. *Science* (Washington, D.C.) **1994**, *265*, 75−79; Huisken, F.; Kaloudis, M.; Kulcke, A.; Voelkel, D. *Infrared Phys. Technol*. **1995**, *36*, 171.

(3) Zhelyaskov, V.; Georgiev, G.; Nicolov, Zh. *J. Raman Spectrosc.* **1988**, *19*, 405−412.

(4) Kustanovich, I.; Goldfarb, D. *J. Phys. Chem.* **1991**, *95*, 8818−8823.

(5) Narten, A. H.; Danford, M. D.; Levy, H. A. *Discuss. Faraday Soc*. **1967**, *43*, 97−107.

(6) Soper, A. K.; Phillips, M. G. *Chem. Phys.* **1986**, *107*, 47−55; Vernon, M. F. *J. Chem. Phys.* **1982**, *77*, 47; Page, R. H.; Frey, J. G.; Chen, Y.-R.; Lee, Y. T. *Chem. Phys. Lett.* **1984**, *106*, 373.

(7) Pelmenschikov, A. G.; van Santen, R. A. *J. Phys. Chem.* **1993**, *97*, 10678−10680.

(8) Hermansson, K.; Ojamäe, L. *Int. J. Quantum Chem.* **1992**, *42*, 1251−1270.

(9) Ahlström, P.; Wallquist, A.; Engström, S.; Jönnson, B. *Mol. Phys.* **1989**, *68*, 563−581.

(10) Allen, M. P.; Tildesley, D. J. *Computer Simulation of Liquids*; University Press: New York, 1987.
(11) Wilson, S. T.; Lok, B. M.; Messina, C. A.; Cannan, T. R.; Flaningen, E. M. *J. Am. Chem. Soc*. **1982**, *104*, 1146−1147.
(12) Flanigen, E. M.; Parron, R. L.; Wilson, S. T. *Stud. Surf. Sci. Catal.* **1988**, *37*, 13−27.
(13) Breck, D. W. *Zeolite Molecular Sieves: Structure, Chemistry, and Use;* John Wiley and Sons: New York, 1973.
(14) Leherte, L.; Andre, J.-M.; Vercauteren, D. P.; Derouane, E. G. *J. Mol. Catal.* **1989**, *54*, 426−438.
(15) Lee, S. H.; Moon, G. K.; Choi, S. G.; Kim, H. S. *J. Phys. Chem.* **1994**, *98*, 1561−1569.
(16) Rudolf, P. R.; Crowder; C. E. *Zeolites* **1990**, *10*(3), 163−168.
(17) Kniep, R.; Mootz, D. *Acta Crystallogr., Sect. B* 1973, *B29*, 2292−2294.
(18) Pluth, J. J.; Smith, J. V. *Acta Crystallogr., Sect. C* **1986**, *C42*, 1118−1120.
(19) McCusker, L. B.; Baerlocher, Ch.; Jahn, E.; Bülow, M. *Zeolites* **1991**, *11*, 308−313.
(20) Martens, J. A.; Geerts, H.; Grobet, P. J.; Jacobs, P. A. Zeolite Microporous Solids **1992**, 477−491.
(21) Richardson Jr., J. W.; Vogt, E. T. C. Zeolites, **1992**, *12*, 13−19.
(22) Akporiaye, D.; Stöcker, M. Proceedings of the 9th International Zeolites Conference, Montreal, 1991; p B34.
(23) Sorby, K.; Szostak, R.; Ulan, J. G.; Gronsky, R. *Catal. Lett.* **1990**, *6*, 209−214.
(24) Duncan, B.; Szostak, R.; Sorby, K.; Ulan, J. G. *Catal. Lett*. **1990**, *7*, 367−376.
(25) Duncan, B.; Stöcker, M.; Gwinnup, D.; Szostak, R.; Vinje, K. *Bull. Soc. Chim. Fr.* **1992**, *129*, 98−110.
(26) d'Yvoire, F. *Bull. Soc. Chim. Fr. (II)* **1961**, 1762−1776.
(27) Schmidt, W.; Schüth, F.; Reichert, H.; Unger, K. K.; Zibrowius, B. *Zeolites* **1992**, *12*, 2−8.
(28) Liu, X.; He, H.; Klinowski, J. *J. Phys. Chem.* **1991**, *95*, 9924−9928.
(29) Holmes, A. J.; Kirby, S. J.; Ozin, G. A.; Young, D. *J. Phys. Chem.* **1994**, *98*, 4677−4682.
(30) Pimentel, A.; McClellan, L. *The Hydrogen Bond;* Freeman: San Francisco, 1960.
(31) Pore, J. C.; Texeira, J. *Hydrogen-Bonded Liquids;* Kluwer: Dordrecht, Netherlands, 1991.
(32) Sivakumar, T. C.; Rice, S. A.; Sceats, M. G. *J. Chem. Phys.* **1978**, *69*, 3468−3476.
(33) Bergen, M. S.; Schuh, D.; Sceats, M. G. *J. Chem. Phys.* **1978**, *69*, 3477−3485.
(34) Zhelyaskov, V.; Georgiev, G.; Nicolov, Zh.; Miteva, M. *J. Raman Spectrosc.* **1989**, *20*, 67−75.
(35) Georgiev, G.; Nicolov, Zh.; Zhelyaskov, V.; Miteva, M. *J. Mol. Liq.* **1990**, *45*, 45−48.
(36) Li, J.; Ross, D. K. *Nature (London)* **1993**, *365*, 327−329.
(37) Suzuki, S.; Green, P. G.; Bumgarner, R.; Dasgupta, S.; Goddard, W.; Blake, G. *Science (Washington, D.C.)* **1992**, *257*, 942−945; Liu, K.; Cruzan, J. D.; Saykally, R. J. *Science (Washington, D.C.)* **1996**, *271*, 62, 929.
(38) Mortier, W. J.; Ghosh, S. K.; Shankar, S. *J. Am. Chem. Soc*. **1986**, *108*, 4315−4320.
(39) Van Genechten, K. A.; Mortier, W. J.; Geerlings, P. *J. Chem. Phys.* **1987**, *86*, 5063−5071.
(40) Baekelandt, B. G. Ph.D. Thesis, Leuven, 1992.
(41) Nalewajski, R. F.; Köster, A. M.; Bredow, T.; Jug, K. *J. Mol. Catal.* **1993**, *82*(2−3), 407−423.
(42) Nalewajski, R. F.; Korchowiec, J.; Zhou, Z. Int. J. Quantum Chem., Quantum Chem. Symp. **1988**, *22*, 349−366.
(43) Nalewajski, R. F.; Korchowiec, J.; Michalak, A. Proceedings (Chemical Science); Gadre, S., Ed., 1997.
(44) Korchowiec, J.; Bredow, T.; Jug, K. *Chem. Phys. Lett.* **1994**, *222*, 58.
(45) Janssens, G. O. A.; Baekelandt, B. G.; Toufar, H.; Mortier, W. J.; Schoonheydt, R. A. *Int. J. Quantum Chem.* **1996**, *56*, 317−326.
(46) Baekelandt, B. G.; Janssens, G. O. A.; Toufar, H.; Mortier, W. J.; Schoonheydt, R. A.; Nalewajski, R. F. *J. Phys. Chem.* **1995**, *99*, 9784−9794.
(47) Davis, M. E.; Montes, C.; Hathaway, P. E.; Arhancet, J. P.; Hasha, D. L. *J. Am. Chem. Soc.* **1989**, *111*, 3919−3924.
(48) d'Yvoire, F. Mém. Soc. Chim. (II), **1961**, 1762−1776.
(49) Parr, R. G.; Yang, W. *Density-Functional Theory of Atoms and Molecules;* Oxford University Press: New York, 1989.
(50) Toufar, H.; Baekelandt, B.; Janssens, G. O. A.; Mortier, W. J.; Schoonheydt. R. A. *J. Phys. Chem.* **1995**, *99*, 13876−13885.
(51) Rudolf, P. R.; Crowder, C. E. *Zeolites* **1990**, *10*, 163−168.
(52) Li, H. X.; Davis, M. E. *J. Chem. Soc., Faraday Trans.* **1993**, *89*, 957−964.
(53) Li, H. X., Davis, M. E. *J. Chem. Soc., Faraday Trans.* **1993**, *89*, 951−956.
(54) Wu, Y.; Chmelka, B. F.; Pines, A.; Davis, M. E.; Grobet, P. J.; Jacobs, P. A. *Nature (London)* **1990**, *346*, 550−552.
(55) ref 1, volume 2, p 84f.
(56) Gutmann, V. *The Donor−Acceptor Approach to Molecular Interactions;* Plenum Press: New York, **1972**; pp 7ff, 76ff.
(57) ref 1, volume 2, p 82f.
(58) Blackwell, C. S.; Patton, L. *J. Phys. Chem.* **1984**, *88*, 6135−6139.
(59) Muller, D.; Grunze, I.; Hallas, E.; Ludwig, G. Z. *Anorg. Allg. Chem.* **1983**, *500*, 80−87.
(60) Cochon, E.; Amoureux, J. P. *Solid State Nucl. Magn. Reson.* **1993**, *2*, 205−222.
(61) Grobet, P. J.; Geerts, H.; Martens, J. A.; Jacobs, P. A. *Stud. Surf. Sci. Catal.* **1989**, *52*, 193−201.
(62) Martens, J. A.; Verlinden, B.; Mertens, M.; Grobet, P. J.; Jacobs, P. A. *Zeolite Synthesis;* Occelli, M. L., Robson, H. E., Eds.; *ACS Symposium Series 398;* American Chemical Society: Washington, D.C., 1989; pp 305−328.
(63) Rocha, J.; Liu, X.; Klinowski, J. *Chem. Phys. Lett.* **1991**, *182*, 531−537.
(64) Grobet, P. J.; Kovalakova, M.; Reynders, R.; Geerts, H.; Vulgan, R. *Transact. Technol. Univ. Kosice;* Riecansky Publ: London, 1995; p 1.
(65) Grobet, P. J.; Martens, J. A.; Balakrishnan, I.; Mertens, M.; Jacobs, P. A. *Appl. Catal.* **1989**, *56*, L21−L27.